Supporting Information:

Materials: Skim milk powder, lot 6475, and coagulant, CHY–MAX^{TM} Plus, was provided by Chr. Hansen and used as received. Rhodamine B was purchased from Sigma–Aldrich and dissolved in miliQ water to a concentration of 1.0 % w/w.

Methods: The skim milk powder was reconstituted in 0.5 mg/ml $CaCl_2$ solution, according to IDF standard 157, and left with magnetic stirring for 30 minutes. Dissolved rhodamine was added and the solution was left on a magnetic stirrer for additional 10 minutes covered from light. Hereafter the solution was left at room temperature for 30 minutes and stored in the refrigerator overnight to allow rehydration equilibriums to set in. For microscopy samples the resulting milk solution was incubated on a cleaned glass slide (2 cm in diameter) mounted in a microscope chamber for 1 hour and 30 minutes. The microscope chamber was costume made from Teflon. It is a cylinder (inner diameter of 1.5 cm and total volume ~ 1 ml) tightened against a microscope glass slide (thickness 170 μm). Sample was added from the open top and stirred with a pipette. Incubation was followed by rinsing with a 0.5 mg/ml $CaCl_2$ solution followed by rinsing with a 1000 fold diluted milk solution. The last volume was left in the microscope chamber, chymosin was added to a final concentration of 0.02 international milk–clotting units (IMCU)/ml and mixed carefully. For fluorescence microscopy a Leica AF6000LX inverted microscope was used. Dynamic light scattering experiments were performed on an ALV/CGS–3 instrument at 20°C using samples of 1000 fold diluted milk powder solution in a 0.02 μm filtered $CaCl_2$–solution and with chymosin added to a final concentration of 0.02 IMCU/ml.

Data treatment: In order to check the stability of the sample at low concentration, we used DLS to measure the particle size of nonrenneted CMs over time at the concentrations, C/1, C/100 and C/1000. The data are shown in table 1.

To obtain size histograms the micrographs shown in figure 1D-E and figure 4A-B were analyzed using the ImageJ software (National Health Institute, Bethesda, MD) version 1.41. The particles were located according to the magnitude of their fluorescence intensity and the threshold was adjusted to minimize background noise. Some background noise was inevitable and the threshold was set low to ensure that all the smaller CMs were detected. This results in a small background signal (bars showing < 10 nm in radius in the size distribution histograms) and accordingly these peaks have been omitted in the data treatments. Following this, the number of particles was counted and their size was determined according to fluorescence intensity. The fluorescence intensity was transformed into radius using the formula for a volume of a sphere and further calibrated according to DLS measurements. For calibration a conversion factor was calculated for time 0 min by dividing the average radius obtained by DLS with the radius in arbitrary units found from the fluorescence intensity. Multiplication of the conversion factor with the radius in arbitrary units found from fluorescence intensity gave the corrected value of the radius in nm. The conversion factor was used for all the size distributions before plotting as a histogram. The histogram was fitted to a double Gaussian function of the type

$$f(x) = A_1 \exp\left(-\left(\frac{(x-x_1)}{w_1}\right)^2\right) + A_2 \exp\left(-\left(\frac{(x-x_2)}{w_2}\right)^2\right)$$

and the area of the peaks were found from integration of the separate peaks. The resulting values are seen in table 2.

The fluorescence intensity profiles as seen in figure 1F was extracted directly from the microscope software and background noise was subtracted before further use. The profiles were fitted to the mono–exponential function

$$y = y_0 + A\,(1 - \exp(-k(x+x_0)))$$

that gave the rate constant k of the growth process. The value of the rate constants for the shown fits are 0.1 ± 0.002 min^{-1}, 0.05 ± 0.01 min^{-1} and 0.07 ± 0.002 min^{-1} respectively.

To calculate the number of collisions s^{-1} (Φ) an immobilized CM experiences with diffusing CM from the solution we used the expression given in reference 19

$$\Phi = k_{diff}\, C = 4 D_{CM}\, R\, C$$

where k_{diff} is the diffusion limited rate constant, C is the concentration of CMs, R is the average radius of CMs (immobilized or in solution) and D_{CM} is the diffusion coefficient of the CMs. The stokes-Einstein relation given as

$$D_{CM} = (k_B T)/(6\pi\eta R)$$

determines the diffusion coefficient that we calculated to give the value ~ 1 $\mu m^2 s^{-1}$. Using this diffusion coefficient we found the number of collisions an immobilized CM experiences to be ~ 760 CMs s^{-1} corresponding to $>10^5$ times over a 10 minutes span in lag-times. Out of these $>10^2$ collisions lead to actual aggregation[16]. Having an

approximate value for the rate of successful collisions we used poissonian statistics to predict the distribution of lag-times, assuming that all immobilized CMs reach maturation at the same time. Based on the calculated rate constant of 10.1 min^{-1} we predicted a histogram of lag-times with a peak centered at 10.1 min^{-1} (figure 3B dashed line). For possonian statistics we used the poissonian distribution given by

$$f(x) = (Ak^x e^{-k})/x!$$

where A is a constant. Fitting the experimentally recorded distribution of lag-times to the poissonian distribution (figure 3B full line) yields the most probable aggregation rate to be 0.05 min^{-1}. This value is coherent with the rate constant determined by exponential fitting of the growth traces.

Further investigation of the lag-times showed that the differences are not randomly displaced but that they are related to the increase in intensity and thus the size of the formed aggregates. The relation is showed in figure 3C displaying that longer lag-times leads to aggregation with larger aggregates. The connection between long lag-times and large size increase could be due to continuous aggregation of free CMs in the solution during the long lag-time leaving few or no single CMs behind. However the abrupt size increase is always followed by a slower growth (figure 1F) indicating that several single CMs are diffusing around in the solution.

Table 1. Variation of the average particle size of reconstituted skim milk powder after respectively 10 minutes, 20 minutes, 1 hour, 18 hours and 42 hours after preparation and at concentrations ranging from C/1, C/100 and C/1000. The values shown are an average of at least 3 measurements.

Time	**10 min**	**20 min**	**1 hour**	**18 hours**

C/1 Particle radius (nm)	117.6 ± 12	118.1 ± 2	111.6 ± 7	111.4 ± 3
C/100 Particle radius (nm)	111.1 ± 9	117.3 ± 2	110.5 ± 2	
C/1000 Particle radius (nm)	118.5 ± 4	119.4 ± 3	117.6 ± 8	118.2 ± 4

Table 2. Position and width of the peaks from fits of the size histograms shown in figure 2B–E to the sum of two Gaussian functions after 0 min, 18 min, 24 min and 45 min respectively after enzyme addition.

Peak 1	**x_1 (nm)**	**w_1 (nm)**	**A_{G1} (nm^2)**
0 min	109 ± 1	25 ± 1	198 ± 0.4
18 min	126 ± 1.6	25	159 ± 2
24 min	128 ± 2	25	106 ± 1
45 min	144 ± 3	25	90 ± 1
Peak 2	**x_2 (nm)**	**w_2 (nm)**	**A_{G2} (nm^2)**
18 min	185 ± 21	60 ± 26	49 ± 4
24 min	192 ± 14	90 ± 16	76 ± 2
45 min	215 ± 15	108 ± 18	93 ± 2

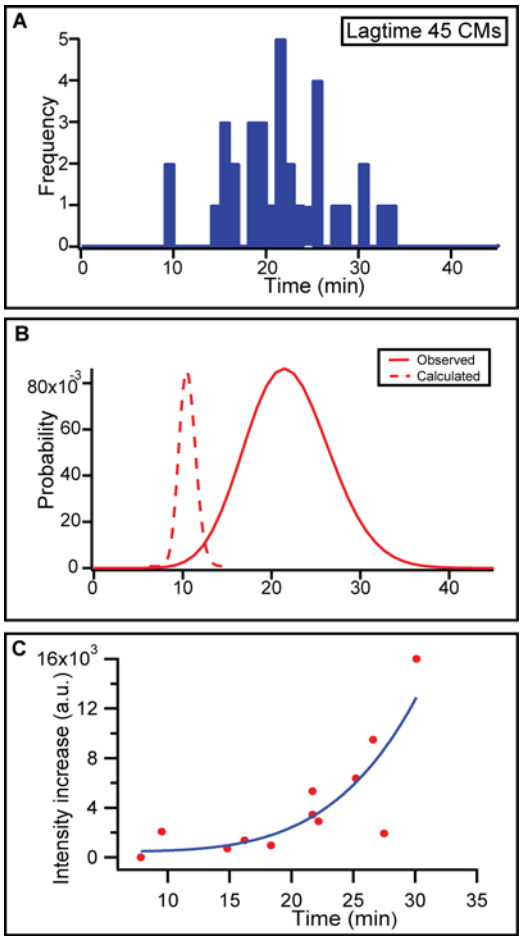

Figure 3. Analysis of the differences in lag-times using poissonian statistics. (A) The distribution of observed lag-times. (B) A poissonian fit of the distribution of observed lag-times (full line) and of the expected lag-times (dashed line). (C) Relation between lag-time and intensity increase. We observed a difference in the lag-time of indivdual CMs as well as a relation between lag-time and size increase. These differences would have been masked out in ensemble averaging measurements such as DLS.

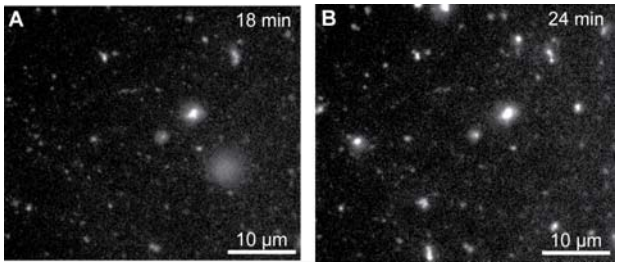

Figure 4. Micrographs of the surface after 18 min and 24 min respectively. These images and the image shown in figure 1D-E have been used to calculate the size distributions shown in figure 2B-E.